

Correlation-driven branch in doped excitonic insulators

Tatsuya Kaneko,¹ Ryota Ueda,¹ and Satoshi Ejima²

¹*Department of Physics, The University of Osaka, Toyonaka, Osaka 560-0043, Japan*

²*Institut für Softwaretechnologie, Abteilung High-Performance Computing,
Deutsches Zentrum für Luft- und Raumfahrt (DLR), 22529 Hamburg, Germany*

(Dated: January 21, 2026)

We investigate the spectral properties of a doped one-dimensional excitonic insulator. Employing matrix-product-state-based methods, we compute the single-particle spectrum and optical conductivity in a correlated two-band model. Our numerical calculation reveals the emergence of a correlation-driven in-gap branch in the doped state. The origin of the in-gap branch is examined by decomposing the propagation dynamics of a single particle, elucidating that the doping-induced branch is associated with excitonic correlations. Our demonstrations suggest that the doping-induced branch can serve as an indicator of electron-hole correlations.

I. INTRODUCTION

Understanding many-body properties in correlated systems is a central issue in condensed matter physics [1, 2]. Excitonic insulators (EIs) are correlation-driven insulators in multiband systems [3–7]. In a semiconductor with a narrow gap or a semimetal with a small band overlap, interband Coulomb interactions modify its electronic structure, and the resulting gap opening leads to an EI state. To date, various candidate materials for EIs have been proposed by both theory and experiment [8–29]. In several candidate materials that undergo structural transitions, such as TiSe_2 and Ta_2NiSe_5 [30, 31], electron-lattice coupling can contribute to the deformations of their electronic structures [32–36], giving rise to controversy over the origin of their phase transitions [37–39]. Given this background, detecting the excitonic contribution to the ground-state configuration is an important challenge in the study of EIs and their candidate materials.

Carrier doping can serve as a means of examining the contribution of correlation effects to the ground-state configuration because band insulators and correlation-driven insulators exhibit distinct behaviors with respect to doping. In noninteracting band insulators where the independent particle picture is valid, carrier doping can be achieved by shifting the Fermi level without deforming their band structures. However, this rigid-band picture is often inapplicable to strongly correlated systems. For example, hole doping into Mott insulators induces changes in the structure of the single-particle spectrum, where the spectral weight transfer from the upper Hubbard band to near the Fermi level and the emergence of the doping-induced in-gap branch, reflecting spin excitation, have been revealed by numerical calculations [40–48]. Since the EI state is also a correlation-driven insulating state, doping-induced band deformation, which is unexpected in conventional band insulators, potentially occurs in EIs.

In this paper, we investigate the effects of carrier doping on a one-dimensional (1D) EI state described in a correlated two-band model. We compute the single-particle spectrum and optical conductivity employing matrix-product-state-based methods. We find the emergence of

the doping-induced in-gap branch in the single-particle spectrum. In the optical conductivity, the original peak structure based on interband transitions is maintained, while the Drude weight grows with doping, corresponding to the change of the single-particle spectrum. The decomposition of the single-particle dynamics reveals that the doping-induced branch is associated with excitonic correlations.

The rest of this paper is organized as follows. In Sec. II, we introduce our target system, the spectral functions, and the numerical techniques employed in this study. In Sec. III, we present the calculated single-particle spectrum, optical conductivity, and excitonic correlation function. A summary of our study is given in Sec. IV.

II. MODEL AND METHOD

A. Model

To describe an EI state, we employ the simplest correlated two-band model [49–55] whose 1D Hamiltonian is given by

$$\hat{H} = - \sum_j \sum_\alpha t_\alpha \left(\hat{c}_{j,\alpha}^\dagger \hat{c}_{j+1,\alpha} + \text{H.c.} \right) + \frac{D}{2} \sum_j (\hat{n}_{j,a} - \hat{n}_{j,b}) + U \sum_j \hat{n}_{j,a} \hat{n}_{j,b}. \quad (1)$$

$\hat{c}_{j,\alpha}^\dagger$ ($\hat{c}_{j,\alpha}$) is the creation (annihilation) operator of a spinless fermion in orbital α ($= a, b$) at site j . t_α is the hopping parameter between nearest-neighboring sites on orbital α . D is the energy level difference between two orbitals. U is the interorbital Coulomb interaction. We consider the direct-gap type band structure with $t_a t_b < 0$. In this paper, $t_a = t_h$ (> 0) is the unit of energy. We set $t_b = -t_a$ unless otherwise specified. Throughout the paper, the Planck constant (\hbar), the charge of a particle (e), and the lattice constant are set to 1. The number of lattice sites and the number of fermions are denoted by L and N , respectively. $N = N_a + N_b$, where N_α is

the number of fermions in orbital α . We address the case where $D > 0$ and $N_b > N_a$. When $U = 0$ without doping, the a -orbital chain forms the conduction band (CB), and the b -orbital chain forms the valence band (VB). We consider hole doping away from half filling ($N = L$) and define the doping concentration as $\delta = 1 - N/L$.

B. Spectral functions

We compute the single-particle spectrum to visualize the band structure in the correlated model. The single-particle spectrum $A(k, \omega)$ is obtained by the Fourier transformation of the retarded Green's function $G^R(i - j, t - t') = -i\theta(t - t') \sum_\alpha \langle \psi_0 | \{\hat{c}_{i,\alpha}(t), \hat{c}_{j,\alpha}^\dagger(t')\} | \psi_0 \rangle$, where $|\psi_0\rangle$ is the ground state, $\theta(t)$ is the step function, and $\hat{O}(t) = e^{i\hat{H}t} \hat{O} e^{-i\hat{H}t}$ for an operator \hat{O} . In our numerical calculations using finite-size systems, the following two functions are computed:

$$G_\alpha^+(x, t) = -i \langle \psi_0 | \hat{c}_{j_0+x,\alpha}(t) \hat{c}_{j_0,\alpha}^\dagger(0) | \psi_0 \rangle, \quad (2)$$

$$G_\alpha^-(x, t) = -i \langle \psi_0 | \hat{c}_{j_0,\alpha}^\dagger(0) \hat{c}_{j_0+x,\alpha}(t) | \psi_0 \rangle, \quad (3)$$

where $t > 0$ and $j_0 = L/2$. G_α^+ (G_α^-) describes the dynamical properties of a fermion above (below) the Fermi level E_F . The Fourier transformation of $G_\alpha(x, t) = G_\alpha^+(x, t) + G_\alpha^-(x, t)$ is conducted by

$$G_\alpha(k, \omega) = \sum_x e^{-ikx} \int_0^\infty dt e^{i(\omega+i\eta)t} G_\alpha(x, t). \quad (4)$$

η is introduced to perform numerical integrations using data from finite-time simulations up to t_{\max} instead of $t \rightarrow \infty$. The single-particle spectrum of component α is given by

$$A_\alpha(k, \omega) = -\frac{1}{\pi} \text{Im} G_\alpha(k, \omega). \quad (5)$$

The total single-particle spectrum is given by $A(k, \omega) = \sum_\alpha A_\alpha(k, \omega)$.

We also consider the optical conductivity $\sigma(\omega)$. In this paper, the optical conductivity is computed by

$$\sigma(\omega) = \frac{\kappa_T + \chi_{JJ}(\omega)}{i(\omega + i\eta)}. \quad (6)$$

$\kappa_T = \langle \psi_0 | \hat{T} | \psi_0 \rangle / L$ with $\hat{T} = -\sum_{j,\alpha} t_\alpha (\hat{c}_{j,\alpha}^\dagger \hat{c}_{j+1,\alpha} + \text{H.c.})$ corresponds to the kinetic energy. $\chi_{JJ}(\omega)$ is the dynamical current-current correlation function

$$\chi_{JJ}(\omega) = \frac{i}{L} \int_0^\infty dt e^{i(\omega+i\eta)t} \langle \psi_0 | [\hat{J}(t), \hat{J}(0)] | \psi_0 \rangle, \quad (7)$$

where $\hat{J} = -i \sum_{j,\alpha} t_\alpha (\hat{c}_{j,\alpha}^\dagger \hat{c}_{j+1,\alpha} - \text{H.c.})$ is the current operator.

C. Method

We employ the density-matrix renormalization group (DMRG) method [56–58] to obtain the ground state $|\psi_0\rangle$. The ground-state properties of the nondoped insulating state have been investigated by the previous DMRG calculation in Ref. [59]. We use the 1D chain of $L = 160$ sites with open boundary conditions. In the present model, $M = N_b - N_a$ can be a quantum number. We evaluate the energy as a function of M and employ the state with the lowest energy as the ground state. The bond dimension for the ground-state calculation is up to $m = 2000$, where the largest truncation error is less than 10^{-10} . We evolve the system in real time using the time-evolving block decimation (TEBD) algorithm [60] to obtain dynamical correlation functions. The time evolution is carried out using the second-order Suzuki-Trotter decomposition [61]. The time step $\delta t = 0.01/t_h$ and the bond dimension $m = 1000$ are used for time evolutions up to $t_{\max} = 40/t_h$. The damping factor, which gives Lorentzian broadening in the spectral functions, is $\eta = 0.125t_h$. We employ the window function $w(t) = [1 + \cos(\pi t/t_{\max})]/2$ in the Fourier transformation to reduce artifacts from the finite-time cutoff at t_{\max} [62]. The Fermi level is defined as $E_F = -[E_{\min}(N-1) - E_0(N)]$, where $E_0(N)$ is the ground-state energy of N fermions and $E_{\min}(N-1)$ is the minimum energy when one fermion is removed from the ground-state configuration [63]. In this definition, E_F of the insulating state corresponds to the lower edge of the band gap.

III. RESULTS

A. Single-particle spectrum

Figure 1(a) presents the single-particle spectra of the nondoped state at $U = 3t_h$. In the noninteracting case ($U = 0$), the CB and VB, which are formed by the a and b orbitals, respectively, overlap around the Γ ($k = 0$) point. However, as shown in Fig. 1(a), the band gap opens, and the band edges become flat near the Γ point due to the Coulomb repulsion U . On the flat structure near the Γ point, the spectral weight of the a (b) orbital remains below (above) E_F . This insulating state is purely due to the interband (i.e., excitonic) interaction U , and we regard this state as an EI state in a 1D system. The spectral properties of the nondoped state are consistent with the previous studies [64–66].

The single-particle spectra of the doped state are shown in Fig. 1(b). In addition to the downward shift of E_F , the spectral structure itself is deformed from the nondoped state, indicating that the rigid-band picture is not valid. While the original gap structure due to U seen in the nondoped state remains, the in-gap branch emerges from the lower band, and the doped state becomes metallic. As shown in $A_a(k, \omega)$ [middle panel of Fig. 1(b)], the doping-induced branch stems from the spectral weight of

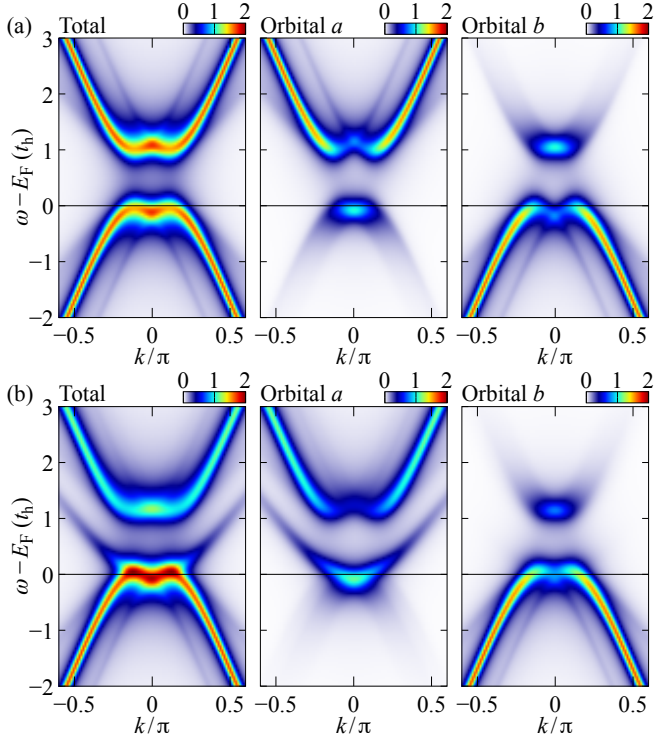


FIG. 1. Single-particle spectra for (a) $\delta = 0$ (half filling) and (b) $\delta = 0.05$ (hole doping), where $U = 3t_h$ and $D = 1.95t_h$. The left, middle, and right panels display $A(k, \omega)$ (total), $A_a(k, \omega)$ (orbital a), and $A_b(k, \omega)$ (orbital b), respectively. The horizontal lines represent the Fermi level E_F .

the a -orbital component and develops above E_F .

As a result of doping, the spectral weight in the upper band decreases and is redistributed to the region near E_F . To clarify the doping-induced spectral-weight transfer, we plot the density of states (DOS) $\rho_\alpha(\omega) = (1/L) \sum_k A_\alpha(k, \omega)$ in Fig. 2, where $\omega = 0$ is set at the center of the gap in the nondoped state ($\delta = 0$). Note that the nonzero weight in the gap of the insulating state at $\delta = 0$ [Fig. 2(a)] is due to the broadening factor η introduced in the numerical calculation. Compared with the nondoped insulating state [Fig. 2(a)], the total DOS in the upper band is suppressed [Fig. 2(b)], while the spectral weights near E_F increase in the doped state. This spectral property is similar to that of Mott insulators [40, 42]. Hence, carrier doping in the 1D EI modifies the structure of the single-particle spectrum, distinguishing it from carrier doping in band insulators described in the rigid-band picture.

B. Optical conductivity

Figure 3 presents the real part of the optical conductivity $\sigma(\omega)$ at $U = 3t_h$. The spectral weight appears above the single-particle gap when $\delta = 0$ (dashed line

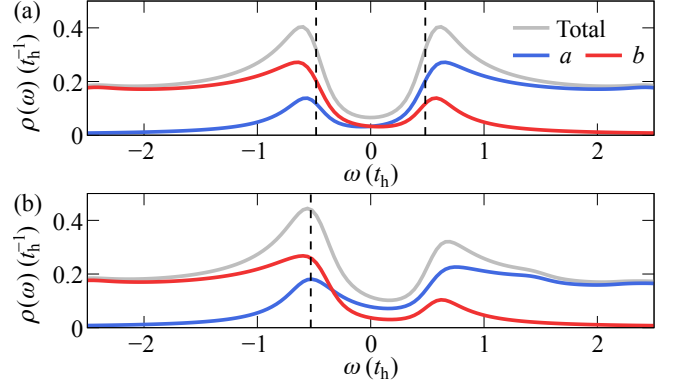


FIG. 2. Densities of states for (a) $\delta = 0$ (half filling) and (b) $\delta = 0.05$ (hole doping), where $U = 3t_h$ and $D = 1.95t_h$. The energy of the horizontal axis is shifted by $U/2$, where the center of the gap is at zero in (a). The vertical dashed lines in (a) indicate the lower and upper edges of the band gap. The vertical dashed line in (b) represents the Fermi level E_F .

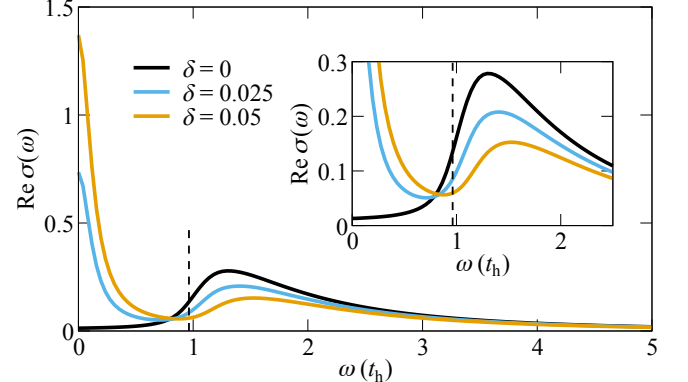


FIG. 3. Real part of the optical conductivity $\sigma(\omega)$ for various δ , where $U = 3t_h$ and $D = 1.95t_h$. The vertical dashed line represents the single-particle excitation gap of the nondoped insulator ($\delta = 0$). Inset: Enlarged view of the spectra. Note that when $\delta = 0$, the nonzero optical conductivity for ω below the gap is due to the broadening factor introduced in the numerical calculation.

in Fig. 3) [67], whereas doping changes the structure of the optical conductivity. First, the peak at $\omega = 0$, corresponding to the Drude weight, grows as the doping δ increases, reflecting the metallic nature of the doped state, which is consistent with the single-particle spectrum shown in Fig. 1(b). Second, the peak structure above the gap when $\delta = 0$ (dashed line in Fig. 3) remains even with hole doping, while its spectral weight decreases. These remnants of the gap structure are consistent with the single-particle spectral features of the doped state shown in Fig. 1(b), indicating that the optical conductivity $\sigma(\omega)$ captures both the metallic nature and the band structure of the doped EI.

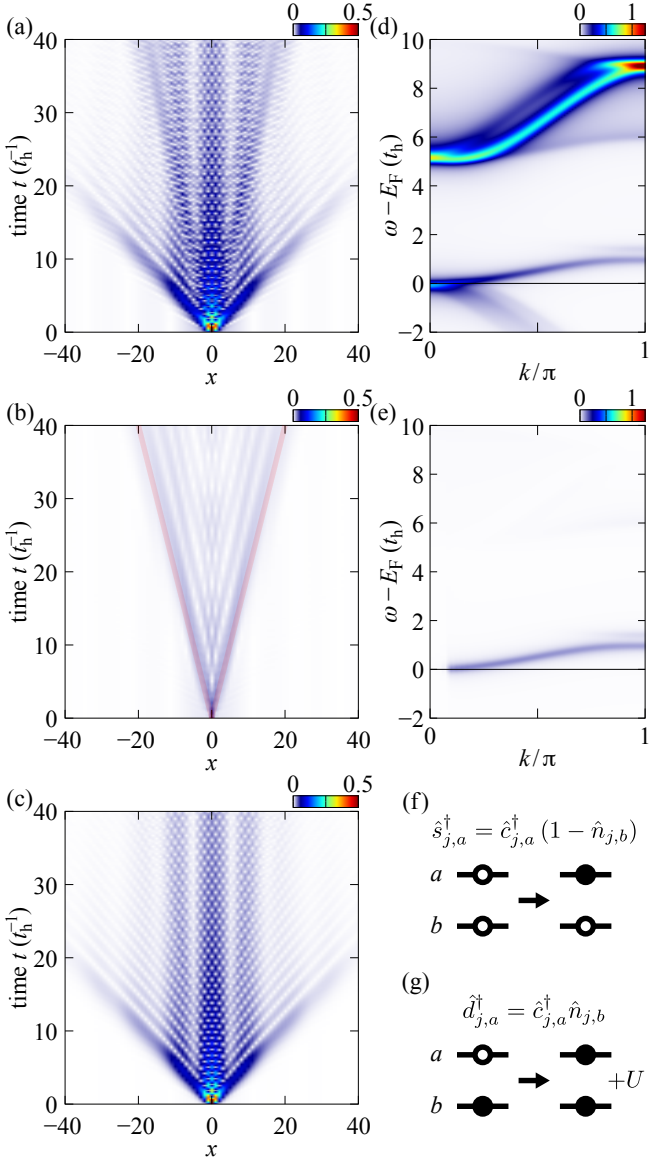


FIG. 4. Absolute values of the space-time correlation functions $\mathcal{G}_a(x, t) = -i \langle \psi_0 | \hat{O}_{j+x,a}(t) \hat{O}_{j,a}^\dagger(0) | \psi_0 \rangle$ for (a) $\hat{O}_{j,a}^\dagger = \hat{c}_{j,a}^\dagger$, (b) $\hat{O}_{j,a}^\dagger = \hat{s}_{j,a}^\dagger = \hat{c}_{j,a}^\dagger(1 - \hat{n}_{j,b})$, and (c) $\hat{O}_{j,a}^\dagger = \hat{d}_{j,a}^\dagger = \hat{c}_{j,a}^\dagger \hat{n}_{j,b}$, where $U = 8t_h$, $D = 0.92t_h$, and $\delta = 0.05$. The translucent red lines in (b) represent $x = \pm Jt$, where $J = 4t_a t_b / U$. (d) Single-particle spectrum $A_a(k, \omega)$ and (e) spectrum obtained by the Fourier transformation of $\mathcal{G}_a(x, t)$ for $\hat{s}_{j,a}^\dagger$ in (b). Schematic figures of the operators (f) $\hat{s}_{j,a}^\dagger = \hat{c}_{j,a}^\dagger(1 - \hat{n}_{j,b})$ and (g) $\hat{d}_{j,a}^\dagger = \hat{c}_{j,a}^\dagger \hat{n}_{j,b}$.

C. Origin of the doping-induced branch

Let us now discuss the origin of the doping-induced branch seen in Fig. 1(b). Since the branch grows above E_F in the a -orbital component [middle panel of Fig. 1(b)], we consider $G_a^+(x, t) = -i \langle \psi_0 | \hat{c}_{j+x,a}(t) \hat{c}_{j,a}^\dagger(0) | \psi_0 \rangle$, which describes the propagation of a created fermion along the

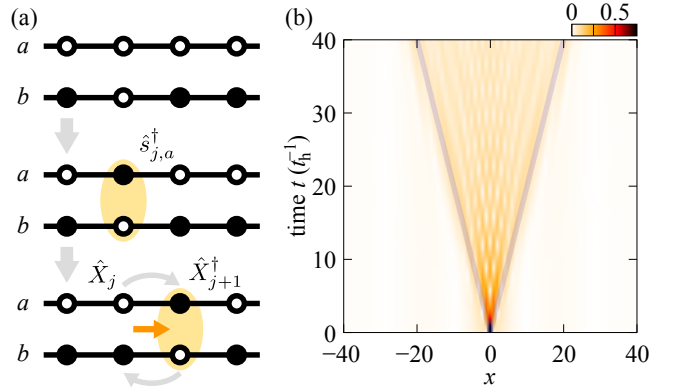


FIG. 5. (a) Schematic figure of the single-particle creation and the propagation of the created particle along the a -orbital chain. (b) Absolute value of the correlation function $\mathcal{G}_X(x, t) = -i \langle \psi_0 | \hat{X}_{j+x}(t) \hat{X}_j^\dagger(0) | \psi_0 \rangle$ for $\hat{X}_j^\dagger = \hat{c}_{j,a}^\dagger \hat{c}_{j,b}$, where $U = 8t_h$, $D = 0.92t_h$, and $\delta = 0.05$. The translucent blue lines in (b) represent $x = \pm Jt$, where $J = 4t_a t_b / U$.

a -orbital chain. In this function, there are two possible processes for the creation of a fermion in the a -orbital chain: (I) creation with an empty b orbital [Fig. 4(f)] and (II) creation with an occupied b orbital [Fig. 4(g)]. To account for these processes, we decompose the creation operator as

$$\hat{c}_{j,a}^\dagger = \hat{c}_{j,a}^\dagger(1 - \hat{n}_{j,b}) + \hat{c}_{j,a}^\dagger \hat{n}_{j,b} = \hat{s}_{j,a}^\dagger + \hat{d}_{j,a}^\dagger, \quad (8)$$

where $\hat{s}_{j,a}^\dagger$ corresponds to the creation of a singly occupied site [case (I), Fig. 4(f)] while $\hat{d}_{j,a}^\dagger$ represents the creation of a doubly occupied site [case (II), Fig. 4(g)]. Here, we demonstrate the propagation dynamics of an a -orbital fermion using the operators $\hat{s}_{j,a}^\dagger$ and $\hat{d}_{j,a}^\dagger$.

Figures 4(a)–4(c) show the absolute values of the space-time correlation functions $\mathcal{G}_a(x, t) = -i \langle \psi_0 | \hat{O}_{j+x,a}(t) \hat{O}_{j,a}^\dagger(0) | \psi_0 \rangle$ for $\hat{O}_{j,a}^\dagger = \hat{c}_{j,a}^\dagger$, $\hat{s}_{j,a}^\dagger$, and $\hat{d}_{j,a}^\dagger$. Here, $U = 8t_h$ is used to differentiate the energy scale of the doping-induced branch from others. In the large- U regime, the correlators with different components, e.g., $\langle \psi_0 | \hat{s}_{j+x,a}(t) \hat{d}_{j,a}^\dagger(0) | \psi_0 \rangle$, gives minor contributions. As seen in Fig. 4(c), the broad propagation feature in Fig. 4(a) is reproduced by $\hat{d}_{j,a}^\dagger$. However, the slow propagation line, which is absent in Fig. 4(c), arises from the $\hat{s}_{j,a}^\dagger$ contribution as shown in Fig. 4(b). In Figs. 4(d) and 4(e), the single-particle spectrum $A_a(k, \omega)$ is compared with the spectral function obtained by $\mathcal{G}_a(x, t)$ associated with $\hat{s}_{j,a}^\dagger$. As shown in Fig. 4(e), the spectrum for $\hat{O}_{j,a}^\dagger = \hat{s}_{j,a}^\dagger$ only constructs the low-energy branch near E_F . Although it is a partial contribution of the spectral weights in $A_a(k, \omega)$, the essential spectral structure of the in-gap branch near E_F is mainly constructed by the contribution of $\hat{s}_{j,a}^\dagger$. On the other hand, since $\hat{d}_{j,a}^\dagger$ creates a fermion with the energy

increase of U [see Fig. 4(g)], the upper band away from E_F in Fig. 4(d) is mainly attributed to the dynamical properties described by $\hat{d}_{j,a}^\dagger$. Therefore, the propagation of a fermion created by case (I) [Fig. 4(f)] causes the emergence of the doping-induced branch near E_F .

Figure 5(a) schematically shows the propagation dynamics of a fermion created by $\hat{s}_{j,a}^\dagger$. Since the ground state is hole-doped, there are unoccupied sites, in which both a and b orbitals are empty [top panel in Fig. 5(a)]. The operator $\hat{s}_{j,a}^\dagger = \hat{c}_{j,a}^\dagger(1 - \hat{n}_{j,b})$ creates a fermion on an a orbital when the other orbital is empty [middle panel in Fig. 5(a)]. Then, the created fermion begins to propagate along the a -orbital chain. However, the motion of the created fermion is not simply allowed by the free hopping t_a due to the Coulomb repulsion U . Particularly, in the large- U case ($U \gg t_a, t_b$), the motion of a fermion along the a -orbital chain is strongly coupled to the motion of a hole along the b -orbital chain to avoid the creation of a doubly occupied site. In this case, the propagation of the created fermion is allowed by the particle exchange process shown in the bottom panel of Fig. 5(a). This second-order process is characterized by the energy of $J = 4t_a t_b / U$. When the creation operator of a local exciton is defined as $\hat{X}_j^\dagger = \hat{c}_{j,a}^\dagger \hat{c}_{j,b}$, the second-order particle exchange process is described by $J \hat{X}_{j+1}^\dagger \hat{X}_j$. Hence, the particle propagation along the a -orbital chain can be characterized by the excitonic operator \hat{X}_j . To demonstrate its dynamics, we present the space-time correlation function $\mathcal{G}_X(x, t) = -i \langle \psi_0 | \hat{X}_{j+x}(t) \hat{X}_j^\dagger(0) | \psi_0 \rangle$ in Fig. 5(b). The time scale of the excitonic propagation in Fig. 5(b) is consistent with that for the a -orbital fermion shown in Fig. 4(b). The lines in Fig. 5(b), which represent the slope of the propagation of $\mathcal{G}_X(x, t)$, are characterized by J . The slope occurring in $\mathcal{G}_X(x, t)$ [Fig. 5(b)] is in good agreement with that for the fermion propagation in Fig. 4(b). This correspondence indicates that the doping-induced branch, which is obtained by the Fourier transformation of $\mathcal{G}_a(x, t)$ in Fig. 4(b), can reflect the excitonic correlation.

IV. SUMMARY AND OUTLOOK

We investigated the spectral properties of a doped EI. Employing the matrix-product-state-based methods, we computed the spectral functions in the correlated two-band model. We found the emergence of the doping-induced in-gap branch in the single-particle spectrum. This spectral property is contrasted to conventional band insulators, in which carrier doping is achieved without deforming their band structures. In the optical conduc-

tivity, the spectral structure at $\omega > 0$ of the nondoped state is maintained, while the Drude weight is generated with doping. We examined the origin of the doping-induced branch using the projected fermion operators. We revealed that the doping-induced branch is strongly associated with the excitonic correlation. Our findings suggest that the doping-induced branch can serve as an indicator of the electron-hole correlation.

In this paper, we used the hopping amplitude t_h as the unit of energy. If we set $t_h \sim 0.3$ eV, the calculated $\sigma(\omega)$ for the nondoped state in Fig. 3 exhibits a similar spectrum to the optical conductivity of Ta_2NiSe_5 [15, 68]. A more quantitative discussion of Ta_2NiSe_5 , which undergoes a structural transition, requires a spectral evaluation that incorporates electron-lattice coupling because our calculation only considered the electron-electron interaction. Electron-lattice coupling may also influence the occurrence of the doping-induced branch. Carrier doping in bulk samples has been realized by elemental substitution, such as $(\text{Ta}_{1-x}\text{Ti}_x)_2\text{NiSe}_5$ [69]. We expect that the spectral properties of doped EI candidates will be uncovered in the future. Our model assumed that the Coulomb interaction is unaffected by doping, whereas changes in Coulomb interactions due to carrier doping potentially occur. Taking into account screening effects on Coulomb interactions is also quantitatively important when discussing doping in real materials. Since our model [Eq. (1)] is spinless, the pseudospin representation for orbitals a and b maps our two-orbital model to the Hubbard model with spin-dependent hoppings under a Zeeman field. It is therefore natural that the spectral structure changes upon doping, as observed in doped Mott insulators. When spin degrees of freedom are active [70–72], richer branches incorporating spin dynamics can also emerge in doped EIs. These issues are interesting topics for future research.

ACKNOWLEDGMENTS

We thank K. Aido, M. Akiyama, J. Han, Y. Inokuma, T. Kondo, K. Kuroki, R. Mizuno, M. Ochi, Y. Ōno, and S. Tsuchida for fruitful discussions. This work was supported by Grants-in-Aid for Scientific Research from JSPS, KAKENHI Grant No. JP24K06939, No. JP24H00191, and No. JP24K01333. R.U. was supported by the Program for Leading Graduate Schools: “Interactive Materials Science Cadet Program” and JST SPRING, Grant No. JPMJSP2138. This project was made possible by the DLR Quantum Computing Initiative and the Federal Ministry for Economic Affairs and Climate Action; qci.dlr.de/projects/ALQU. The DMRG and TEBD simulations were performed using the ITensor library [73].

[1] M. Imada, A. Fujimori, and Y. Tokura, Metal-insulator transitions, *Rev. Mod. Phys.* **70**, 1039 (1998).

[2] E. Dagotto, Complexity in strongly correlated electronic

systems, *Science* **309**, 257 (2005).

[3] L. V. Keldysh and Y. V. Kopeav, Possible instability of the semimetallic state toward Coulomb interaction, *Sov. Phys. Solid State* **6**, 2219 (1965).

[4] J. D. Cloizeaux, Exciton instability and crystallographic anomalies in semiconductors, *J. Phys. Chem. Solids* **26**, 259 (1965).

[5] D. Jérôme, T. M. Rice, and W. Kohn, Excitonic insulator, *Phys. Rev.* **158**, 462 (1967).

[6] B. I. Halperin and T. M. Rice, Possible anomalies at a semimetal-semiconductor transition, *Rev. Mod. Phys.* **40**, 755 (1968).

[7] T. Kaneko and Y. Ohta, A new era of excitonic insulators, *J. Phys. Soc. Jpn.* **94**, 012001 (2025).

[8] M. M. Traum, G. Margaritondo, N. V. Smith, J. E. Rowe, and F. J. Di Salvo, TiSe_2 : Semiconductor, semimetal, or excitonic insulator, *Phys. Rev. B* **17**, 1836 (1978).

[9] H. Cercellier, C. Monney, F. Clerc, C. Battaglia, L. Despont, M. G. Garnier, H. Beck, P. Aebi, L. Patthey, H. Berger, and L. Forró, Evidence for an excitonic insulator phase in $1T\text{-TiSe}_2$, *Phys. Rev. Lett.* **99**, 146403 (2007).

[10] A. Kogar, M. S. Rak, S. Vig, A. A. Husain, F. Flicker, Y. I. Joe, L. Venema, G. J. MacDougall, T. C. Chiang, E. Fradkin, J. van Wezel, and P. Abbamonte, Signatures of exciton condensation in a transition metal dichalcogenide, *Science* **358**, 1314 (2017).

[11] Q. Gao, Y.-h. Chan, P. Jiao, H. Chen, S. Yin, K. Tangrapha, Y. Yang, X. Li, Z. Liu, D. Shen, S. Jiang, and P. Chen, Observation of possible excitonic charge density waves and metal-insulator transitions in atomically thin semimetals, *Nat. Phys.* **20**, 597 (2024).

[12] Y. Wakisaka, T. Sudayama, K. Takubo, T. Mizokawa, M. Arita, H. Namatame, M. Taniguchi, N. Katayama, M. Nohara, and H. Takagi, Excitonic insulator state in Ta_2NiSe_5 probed by photoemission spectroscopy, *Phys. Rev. Lett.* **103**, 026402 (2009).

[13] K. Seki, Y. Wakisaka, T. Kaneko, T. Toriyama, T. Konishi, T. Sudayama, N. L. Saini, M. Arita, H. Namatame, M. Taniguchi, N. Katayama, M. Nohara, H. Takagi, T. Mizokawa, and Y. Ohta, Excitonic Bose-Einstein condensation in Ta_2NiSe_5 above room temperature, *Phys. Rev. B* **90**, 155116 (2014).

[14] T. Yamada, K. Domon, and Y. Ōno, FFLO excitonic state in the three-chain Hubbard model for Ta_2NiSe_5 , *J. Phys. Soc. Jpn.* **85**, 053703 (2016).

[15] Y. F. Lu, H. Kono, T. I. Larkin, A. W. Rost, T. Takayama, A. V. Boris, B. Keimer, and H. Takagi, Zero-gap semiconductor to excitonic insulator transition in Ta_2NiSe_5 , *Nat. Commun.* **8**, 14408 (2017).

[16] K. Kim, H. Kim, J. Kim, C. Kwon, J. S. Kim, and B. J. Kim, Direct observation of excitonic instability in Ta_2NiSe_5 , *Nat. Commun.* **12**, 1969 (2021).

[17] K. Fukutani, R. Stania, C. Il Kwon, J. S. Kim, K. J. Kong, J. Kim, and H. W. Yeom, Detecting photoelectrons from spontaneously formed excitons, *Nat. Phys.* **17**, 1024 (2021).

[18] J. Huang, B. Jiang, J. Yao, D. Yan, X. Lei, J. Gao, Z. Guo, F. Jin, Y. Li, Z. Yuan, C. Chai, H. Sheng, M. Pan, F. Chen, J. Liu, S. Gao, G. Qu, B. Liu, Z. Jiang, Z. Liu, X. Ma, S. Zhou, Y. Huang, C. Yun, Q. Zhang, S. Li, S. Jin, H. Ding, J. Shen, D. Su, Y. Shi, Z. Wang, and T. Qian, Evidence for an excitonic insulator state in $\text{Ta}_2\text{Pd}_3\text{Te}_5$, *Phys. Rev. X* **14**, 011046 (2024).

[19] P. Zhang, Y. Dong, D. Yan, B. Jiang, T. Yang, J. Li, Z. Guo, Y. Huang, Haobo, Q. Li, Y. Li, K. Kurokawa, R. Wang, Y. Nie, M. Hashimoto, D. Lu, W.-H. Jiao, J. Shen, T. Qian, Z. Wang, Y. Shi, and T. Kondo, Spontaneous gap opening and potential excitonic states in an ideal dirac semimetal $\text{Ta}_2\text{Pd}_3\text{Te}_5$, *Phys. Rev. X* **14**, 011047 (2024).

[20] M. S. Hossain, Z.-J. Cheng, Y.-X. Jiang, T. A. Cochran, S.-B. Zhang, H. Wu, X. Liu, X. Zheng, G. Cheng, B. Kim, Q. Zhang, M. Litskevich, J. Zhang, J. Liu, J.-X. Yin, X. P. Yang, J. D. Denlinger, M. Tallarida, J. Dai, E. Vescovo, A. Rajapitamahuni, N. Yao, A. Keselman, Y. Peng, Y. Yao, Z. Wang, L. Balicas, T. Neupert, and M. Z. Hasan, Topological excitonic insulator with tunable momentum order, *Nat. Phys.* **21**, 1250 (2025).

[21] J. Kuneš and P. Augustinský, Excitonic condensation of strongly correlated electrons: The case of $\text{Pr}_{0.5}\text{Ca}_{0.5}\text{CoO}_3$, *Phys. Rev. B* **90**, 235112 (2014).

[22] A. Ikeda, Y. H. Matsuda, K. Sato, Y. Ishii, H. Sawabe, D. Nakamura, S. Takeyama, and J. Nasu, Signature of spin-triplet exciton condensations in LaCoO_3 at ultrahigh magnetic fields up to 600 T, *Nat. Commun.* **14**, 1744 (2023).

[23] D. Varsano, M. Palummo, E. Molinari, and M. Rontani, A monolayer transition-metal dichalcogenide as a topological excitonic insulator, *Nat. Nanotech.* **15**, 367 (2020).

[24] Y. Jia, P. Wang, C.-L. Chiu, Z. Song, G. Yu, B. Jäck, S. Lei, S. Klemenz, F. A. Cevallos, M. Onyszczak, N. Fishchenko, X. Liu, G. Farahi, F. Xie, Y. Xu, K. Watanabe, T. Taniguchi, B. A. Bernevig, R. J. Cava, L. M. Schoop, A. Yazdani, and S. Wu, Evidence for a monolayer excitonic insulator, *Nat. Phys.* **18**, 87 (2022).

[25] B. Sun, W. Zhao, T. Palomaki, Z. Fei, E. Runburg, P. Malinowski, X. Huang, J. Cenker, Y.-T. Cui, J.-H. Chu, X. Xu, S. S. Ataei, D. Varsano, M. Palummo, E. Molinari, M. Rontani, and D. H. Cobden, Evidence for equilibrium exciton condensation in monolayer WTe_2 , *Nat. Phys.* **18**, 94 (2022).

[26] B. Bucher, P. Steiner, and P. Wachter, Excitonic insulator phase in $\text{TmSe}_{0.45}\text{Te}_{0.55}$, *Phys. Rev. Lett.* **67**, 2717 (1991).

[27] D. G. Mazzone, Y. Shen, H. Suwa, G. Fabbris, J. Yang, S. S. Zhang, H. Miao, J. Sears, K. Jia, Y. G. Shi, M. H. Upton, D. M. Casa, X. Liu, J. Liu, C. D. Batista, and M. P. M. Dean, Antiferromagnetic excitonic insulator state in $\text{Sr}_3\text{Ir}_2\text{O}_7$, *Nat. Commun.* **13**, 913 (2022).

[28] H. Qu, H. Liu, and Y. Li, First-principles design of excitonic insulators: A review, *Chinese Phys. B* **34**, 097101 (2025).

[29] R. Okuma, K. Yamagami, Y. Fujisawa, C. H. Hsu, Y. Obata, N. Tomoda, M. Dronova, K. Kuroda, H. Ishikawa, K. Kawaguchi, K. Aido, K. Kindo, Y. H. Chan, H. Lin, Y. Ihara, T. Kondo, and Y. Okada, Emergent topological magnetism in Hund's excitonic insulator, *arXiv:2405.16781*.

[30] F. J. Di Salvo, D. E. Moncton, and J. V. Waszczak, Electronic properties and superlattice formation in the semimetal TiSe_2 , *Phys. Rev. B* **14**, 4321 (1976).

[31] F. Di Salvo, C. Chen, R. Fleming, J. Waszczak, R. Dunn, S. Sunshine, and J. A. Ibers, Physical and structural properties of the new layered compounds Ta_2NiS_5 and Ta_2NiSe_5 , *J. Less Common Met.* **116**, 51 (1986).

[32] J. van Wezel, P. Nahai-Williamson, and S. S. Saxena, Exciton-phonon-driven charge density wave in TiSe_2 ,

Phys. Rev. B **81**, 165109 (2010).

[33] C. Monney, G. Monney, P. Aebi, and H. Beck, Electron-hole fluctuation phase in 1T-TiSe₂, *Phys. Rev. B* **85**, 235150 (2012).

[34] T. Kaneko, T. Toriyama, T. Konishi, and Y. Ohta, Orthorhombic-to-monoclinic phase transition of Ta₂NiSe₅ induced by the Bose-Einstein condensation of excitons, *Phys. Rev. B* **87**, 035121 (2013).

[35] B. Zenker, H. Fehske, and H. Beck, Fate of the excitonic insulator in the presence of phonons, *Phys. Rev. B* **90**, 195118 (2014).

[36] Y. Murakami, D. Golež, T. Kaneko, A. Koga, A. J. Millis, and P. Werner, Collective modes in excitonic insulators: Effects of electron-phonon coupling and signatures in the optical response, *Phys. Rev. B* **101**, 195118 (2020).

[37] Z. Lin, C. Wang, A. Balassis, J. P. Echeverry, A. S. Vasenko, V. M. Silkin, E. V. Chulkov, Y. Shi, J. Zhang, J. Guo, and X. Zhu, Dramatic plasmon response to the charge-density-wave gap development in 1T-TiSe₂, *Phys. Rev. Lett.* **129**, 187601 (2022).

[38] E. Baldini, A. Zong, D. Choi, C. Lee, M. H. Michael, L. Windgaetter, I. I. Mazin, S. Latini, D. Azoury, B. Lv, A. Kogar, Y. Su, Y. Wang, Y. Lu, T. Takayama, H. Takagi, A. J. Millis, A. Rubio, E. Demler, and N. Gedik, The spontaneous symmetry breaking in Ta₂NiSe₅ is structural in nature, *Proc. Natl. Acad. Sci. USA* **120**, e2221688120 (2023).

[39] C. Chen, X. Chen, W. Tang, Z. Li, S. Wang, S. Ding, Z. Kang, C. Jozwiak, A. Bostwick, E. Rotenberg, M. Hashimoto, D. Lu, J. P. C. Ruff, S. G. Louie, R. J. Birgeneau, Y. Chen, Y. Wang, and Y. He, Role of electron-phonon coupling in excitonic insulator candidate Ta₂NiSe₅, *Phys. Rev. Res.* **5**, 043089 (2023).

[40] H. Eskes, M. B. J. Meinders, and G. A. Sawatzky, Anomalous transfer of spectral weight in doped strongly correlated systems, *Phys. Rev. Lett.* **67**, 1035 (1991).

[41] E. Dagotto, F. Ortolani, and D. Scalapino, Single-particle spectral weight of a two-dimensional Hubbard model, *Phys. Rev. B* **46**, 3183 (1992).

[42] M. B. J. Meinders, H. Eskes, and G. A. Sawatzky, Spectral-weight transfer: Breakdown of low-energy-scale sum rules in correlated systems, *Phys. Rev. B* **48**, 3916 (1993).

[43] N. Bulut, D. Scalapino, and S. White, Quasiparticle dispersion in the cuprate superconductors and the two-dimensional Hubbard model, *Phys. Rev. B* **50**, 7215 (1994).

[44] R. Preuss, W. Hanke, and W. von der Linden, Quasiparticle dispersion of the 2D Hubbard model: From an insulator to a metal, *Phys. Rev. Lett.* **75**, 1344 (1995).

[45] D. Sénéchal, D. Perez, and M. Pioro-Ladrière, Spectral weight of the Hubbard model through cluster perturbation theory, *Phys. Rev. Lett.* **84**, 522 (2000).

[46] B. Kyung, S. S. Kancharla, D. Sénéchal, A.-M. S. Tremblay, M. Civelli, and G. Kotliar, Pseudogap induced by short-range spin correlations in a doped Mott insulator, *Phys. Rev. B* **73**, 165114 (2006).

[47] M. Kohno, Spectral properties near the Mott transition in the one-dimensional Hubbard model, *Phys. Rev. Lett.* **105**, 106402 (2010).

[48] M. Kohno, Mott transition in the two-dimensional Hubbard model, *Phys. Rev. Lett.* **108**, 076401 (2012).

[49] C. D. Batista, Electronic ferroelectricity in the Falicov-Kimball model, *Phys. Rev. Lett.* **89**, 166403 (2002).

[50] D. Ihle, M. Pfafferott, E. Burovski, F. X. Bronold, and H. Fehske, Bound state formation and the nature of the excitonic insulator phase in the extended Falicov-Kimball model, *Phys. Rev. B* **78**, 193103 (2008).

[51] K. Seki, R. Eder, and Y. Ohta, BCS-BEC crossover in the extended Falicov-Kimball model: Variational cluster approach, *Phys. Rev. B* **84**, 245106 (2011).

[52] S. Mor, M. Herzog, D. Golež, P. Werner, M. Eckstein, N. Katayama, M. Nohara, H. Takagi, T. Mizokawa, C. Monney, and J. Stähler, Ultrafast electronic band gap control in an excitonic insulator, *Phys. Rev. Lett.* **119**, 086401 (2017).

[53] K. Sugimoto, S. Nishimoto, T. Kaneko, and Y. Ohta, Strong coupling nature of the excitonic insulator state in Ta₂NiSe₅, *Phys. Rev. Lett.* **120**, 247602 (2018).

[54] T. Tanabe, T. Kaneko, and Y. Ohta, Third-harmonic generation in excitonic insulators, *Phys. Rev. B* **104**, 245103 (2021).

[55] A. Osterkorn, Y. Murakami, T. Kaneko, Z. Sun, A. J. Millis, and D. Golež, Optical signatures of dynamical excitonic condensates, *Phys. Rev. Lett.* **135**, 106902 (2025).

[56] S. R. White, Density matrix formulation for quantum renormalization groups, *Phys. Rev. Lett.* **69**, 2863 (1992).

[57] S. R. White, Density-matrix algorithms for quantum renormalization groups, *Phys. Rev. B* **48**, 10345 (1993).

[58] U. Schollwöck, The density-matrix renormalization group in the age of matrix product states, *Ann. Phys.* **326**, 96 (2011).

[59] S. Ejima, T. Kaneko, Y. Ohta, and H. Fehske, Order, criticality, and excitations in the extended Falicov-Kimball model, *Phys. Rev. Lett.* **112**, 026401 (2014).

[60] G. Vidal, Efficient classical simulation of slightly entangled quantum computations, *Phys. Rev. Lett.* **91**, 147902 (2003).

[61] S. Paeckel, T. Köhler, A. Swoboda, S. R. Manmana, U. Schollwöck, and C. Hubig, Time-evolution methods for matrix-product states, *Ann. Phys.* **411**, 167998 (2019).

[62] S. Milner, S. Johnston, and A. Feiguin, Band mixing effects in one-dimensional charge transfer insulators, *arXiv:2508.01011*.

[63] $E_{\min}(N-1) = \min\{E_0(N_a-1, N_b), E_0(N_a, N_b-1)\}$, where $E_0(N_a, N_b)$ is the lowest energy in the (N_a, N_b) sector.

[64] R. Fujiuchi, T. Kaneko, Y. Ohta, and S. Yunoki, Photoinduced electron-electron pairing in the extended Falicov-Kimball model, *Phys. Rev. B* **100**, 045121 (2019).

[65] S. Ejima, F. Lange, and H. Fehske, Finite-temperature photoemission in the extended Falicov-Kimball model: a case study for Ta₂NiSe₅, *SciPost Phys.* **10**, 077 (2021).

[66] S. Ejima, F. Lange, and H. Fehske, Photoinduced metallization of excitonic insulators, *Phys. Rev. B* **105**, 245126 (2022).

[67] Since we do not assume an interorbital dipole [36] whose presence depends on the choice of two orbitals, $\sigma(\omega)$ does not exhibit an in-gap mode at $\delta = 0$.

[68] T. I. Larkin, A. N. Yaresko, D. Pröpper, K. A. Kikoin, Y. F. Lu, T. Takayama, Y.-L. Mathis, A. W. Rost, H. Takagi, B. Keimer, and A. V. Boris, Giant exciton Fano resonance in quasi-one-dimensional Ta₂NiSe₅, *Phys. Rev. B* **95**, 195144 (2017).

[69] S. Tsuchida, Y. Hirose, T. Sekikawa, Y. Ōno, T. Hirahara, S. Sano, S. Kawaguchi, S. Kobayashi, Y. Uwato, and R. Settai, Metallization and pressure-induced

superconductivity in carrier doped excitonic insulator ($\text{Ta}_{1-x}\text{Ti}_x)_2\text{NiSe}_5$, [J. Phys. Soc. Jpn. **94**, 114703 \(2025\)](#)).

[70] J. Kuneš and P. Augustinský, Excitonic instability at the spin-state transition in the two-band Hubbard model, [Phys. Rev. B **89**, 115134 \(2014\)](#).

[71] J. Nasu, T. Watanabe, M. Naka, and S. Ishihara, Phase diagram and collective excitations in an excitonic insulator from an orbital physics viewpoint, [Phys. Rev. B **93**, 205136 \(2016\)](#).

[72] D. Geffroy, J. Kaufmann, A. Hariki, P. Gunacker, A. Hausoel, and J. Kuneš, Collective modes in excitonic magnets: Dynamical mean-field study, [Phys. Rev. Lett. **122**, 127601 \(2019\)](#).

[73] M. Fishman, S. R. White, and E. M. Stoudenmire, The ITensor Software Library for Tensor Network Calculations, [SciPost Phys. Codebases **4** \(2022\)](#).